

Experimental studies on behaviour of bolted ball-cylinder joints under axial force

Xiaonong Guo¹, Zewei Huang¹, Zhe Xiong^{*1}, Shangfei Yang¹ and Li Peng²

¹Department of Building Engineering, Tongji University, Shanghai 200092, China

²Shanghai T&D Architechral Technology Co., Ltd., Shanghai 200092, China

(Received November 10, 2015, Revised February 21, 2016, Accepted March 07, 2016)

Abstract. Due to excellent advantages such as better illuminative effects, considerable material savings and ease and rapidness of construction, the bolted ball-cylinder joint which is a new type joint system has been proposed in space truss structures. In order to reveal more information and understanding on the behaviour of bolted ball-cylinder joints, full-scale experiments on eight bolted ball-cylinder joint specimens were conducted. Five joint specimens were subjected to axial compressive force, while another three joint specimens were subjected to axial tensile force. The parameters investigated herein were the outside diameter of hollow cylinders, the height of hollow cylinders, the thickness of hollow cylinders, ribbed stiffener and axial force. These joint specimens were collapsed by excessive deformation of hollow cylinders, punching damage of hollow cylinders, evulsion of bolts, and weld cracking. The strain distributions on the hollow cylinder opening were mainly controlled by bending moments. To improve the ultimate bearing capacity and axial stiffness of bolted ball-cylinder joints, two effective measures were developed: (1) the thickness of the hollow cylinder needed to be thicker; (2) the ribbed stiffener should be adopted. In addition, the axial stiffness of bolted ball-cylinder joints exhibited significant non-linear characteristics.

Keywords: bolted ball-cylinder joints; full-scale experiments; failure modes; ultimate bearing capacity; axial stiffness

1. Introduction

Due to excellent advantages such as lightness, attractive appearance, high strengths, material savings, etc., space truss structures have been widely used in large span structures. Traditional space truss structures are commonly composed of bolted spherical joints and circular tubes. In the design and analysis of traditional space truss structures, a common practice over the years has assumed that the tube is subjected to axial force. As a result, loads should act on joints to avoid the generation of bending moments. To transfer loads from roof boards to joints, purlines are usually required. However, the purline not only increases the amount of components, but also raises the height of building. Therefore, the main concern of structural designers in recent years has been how to find an appropriate space truss structure system which can resist bending moments and work without purlines. In this respect, a new type joint system, namely a bolted ball-cylinder joint, was proposed. The space truss structure with bolted ball-cylinder joints can overcome these

*Corresponding author, Doctor, E-mail: 123superpanda@tongji.edu.cn

aforementioned drawbacks sufficiently.

The joint is an important component in the space truss structure, as it is supposed to resist resultant force at the end of members and transfer the resultant force to surrounding structural components. Once the joint is fractured, it may lead to the progressive collapse of the entire space truss structure. Thereby, this paper is primarily focused on the mechanical behaviour of bolted ball-cylinder joints.

For the time being, extensive experimental studies and numerical simulations have been performed to investigate the mechanical behaviour of beam-to-column connections which are widely used in frameworks (Daniunas *et al.* 2008, Gil *et al.* 2008a, b, Cabrero *et al.* 2007a, b, Qiang *et al.* 2012a, b, Wang *et al.* 2007, Lima *et al.* 2002, Kattner and Crisinel 2000). Moreover, achievements on the mechanical behaviour of beam-to-column connections are systematical and developed. In comparison with the achievements of beam-to-column connections, the researches of joint systems used in space latticed structures are still developing. A reason for this is that the joint systems are various, including bolt-ball joint system (Ghasemi *et al.* 2010, Ebadi and Davoodi 2012), aluminium alloy gusset joint (Guo *et al.* 2015a, b, 2016a), tubular joint system (Qiu and Zhao 2009, Lesani *et al.* 2013), welded hollow spherical joint system (Wang *et al.* 2000), etc. Through experimental studies and numerical simulations, Fan and Ma *et al.* (Fan *et al.* 2012, Ma *et al.* 2013) had found that socket joints and bolt-ball joints express typical semi-rigid characteristics. Guo and Xiong (Guo *et al.* 2015a, b, 2016a) had carried out systematical studies on the bearing capacities, failure modes and semi-rigid behaviour of aluminium alloy gusset joints. Fung (Fung *et al.* 2001a, b) presented the experimental and numerical findings of the ultimate strengths, load-displacement characteristics and failure mechanisms of completely overlapped tubular joints. Han (Han and Liu 2004) proposed formulae for the resistance of welded hollow balls by means of statistical regression and finite element method. Lopez (Lopez *et al.* 2011) found an appropriate joint design which may be used in single-layer structures, and they presented the results of joint tests conducted with the aim of establishing geometrical parameters. However, the research of bolted ball-cylinder joints is limited, influencing the widespread application and development of bolted ball-cylinder joints greatly.

In this paper and its companion paper, a systematical study on the behaviour of bolted ball-cylinder joints under axial force is investigated. For the effective application and development of bolted ball-cylinder joints in space truss structures, this study is aimed to reveal more information and understanding on the behaviour of bolted ball-cylinder joints. In the present paper, the components of bolted ball-cylinder joints are introduced firstly. Secondly, full-scale tests on eight bolted ball-cylinder joint specimens are conducted to investigate their mechanical behaviour. The parameters investigated herein are the outside diameter of hollow cylinders, the height of hollow cylinders, the thickness of hollow cylinders, ribbed stiffener and axial force. Thirdly, the failure modes of these joint specimens are summarized, and their bearing capacities are discussed. Finally, the strain distributions of hollow cylinder and the axial stiffness of bolted ball-cylinder joints are evaluated.

2. Components of bolted ball-cylinder joints

The components of bolted ball-cylinder joints are plotted in Fig. 1. The bolted ball-cylinder joint is mainly composed of a solid hemisphere, a hollow cylinder, rectangular tubes, circular tubes, concave endplates, convex washers, high strength bolts and ribbed stiffener. The upper

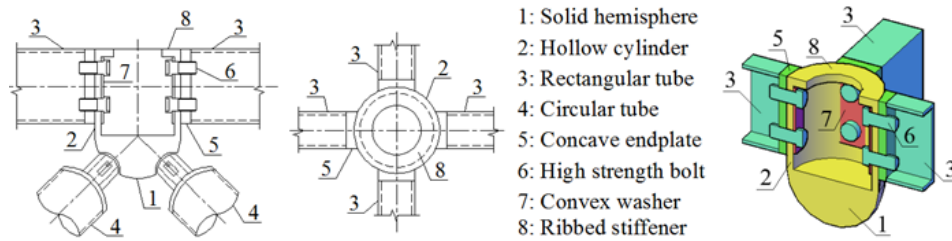


Fig. 1 Components of bolted ball-cylinder joints

portion of bolted ball-cylinder joints is manufactured as a hollow cylinder. The hollow cylinder has an opening and several bolt holes for the insertion of bolts. The dimensions of the hollow cylinder are determined by upper chord members. The lower portion of bolted ball-cylinder joints is a solid hemisphere which belongs to a traditional bolted spherical node. The hollow cylinder and the solid hemisphere are welded together. Rectangular tubes are regarded as upper chord members, while circular tubes are adopted for web members. Each rectangular tube is tightly attached to the hollow cylinder by two high strength bolts. To transmit the axial force smoothly, concave endplates and convex washers are employed. The concave endplates are placed at the outside of the hollow cylinder and the convex washers are placed at the inside of the hollow cylinder. The concave endplates are welded at both ends of the rectangular tubes. The circular tubes are connected with the solid hemisphere through traditional methods. In addition, to enhance the stiffness and the strength of bolted ball-cylinder joints, the ribbed stiffener which is placed at the opening of the hollow cylinder can be considered.

The bolted ball-cylinder joint has an attractive appearance, and the rectangular tubes have a better bending behaviour. Therefore, roof boards can be placed at upper chord members directly. As a result, support brackets and purlines are not required in the space truss structure with bolted ball-cylinder joints. The primary merits of the space truss structure with this new type joint system are concluded as follows: (1) this structure has a better illuminative effect; (2) due to the removal of the support brackets and the purlines, considerable material savings are achieved; (3) the components of bolted ball-cylinder joints could be manufactured in advance, leading to an ease and rapidness of construction. These merits provide a widespread application prospect for the bolted ball-cylinder joint.

3. Experimental program

3.1 Specimens

A series of full-scale tests on eight bolted ball-cylinder joint specimens was conducted to explore their mechanical behaviour. The bolted ball-cylinder joint is usually used in the upper chord of space truss structures. On the one hand, the upper chord members are usually under compressive force in normal practical engineering. Hence, five bolted ball-cylinder joint specimens were subjected to axial compressive force in the tests. On the other hand, the upper chord members may be under tensile force in overhanging space truss structures. Thereby, another three bolted ball-cylinder joint specimens were subjected to axial tensile force in the tests.

In this experimental study, the strengths of these joint specimens were designed on the basis of

GB 50017-2003 (2003). The overall configurations of these joint specimens are plotted in Fig. 2. Each hollow cylinder was connected with four rectangular tubes, and the angle between adjacent tubes is 90 degrees. All the rectangular tubes have the same cross-section of 120×60×5 mm, which represents that the height of the cross-section is 120 mm; the width of the cross-section is 60 mm and the thickness of tube is 5 mm, as shown in Fig. 2(e). The length of long tubes is 116 mm, while the length of short tubes is 56 mm. One loading plate was welded on the end of the

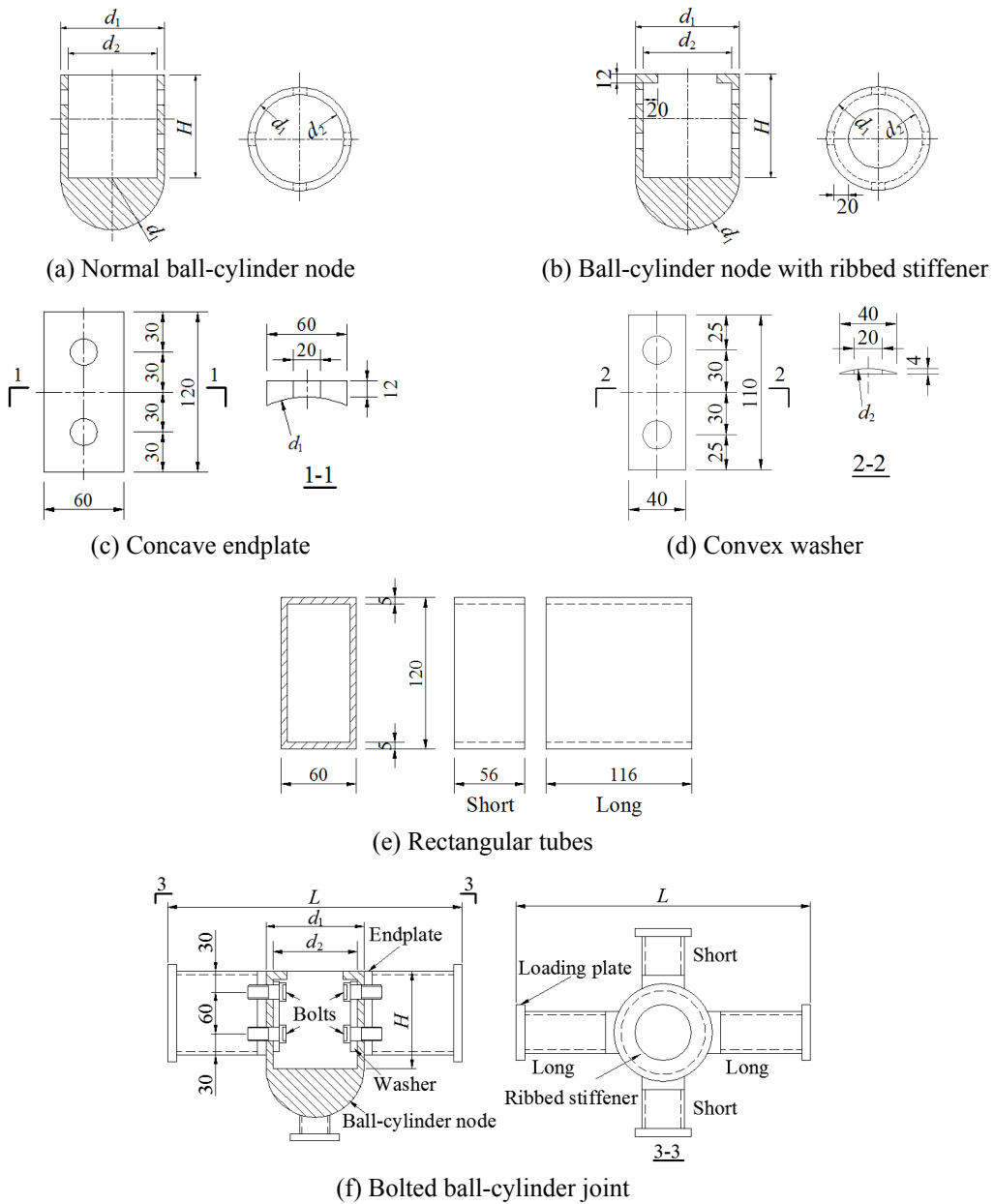


Fig. 2 Configurations of the test specimens

Table 1 Detailed information of the test specimens

No.	d_1 (mm)	d_2 (mm)	H (mm)	Thickness (mm)	Ribbed stiffener	Loading scheme
JD1-H140-T10-RN-C	140	120	140	10	None	Compressive force
JD2-H160-T12-RN-C	140	116	160	12	None	Compressive force
JD3-H120-T12-RN-C	160	136	120	12	None	Compressive force
JD4-H120-T10-RN-C	180	160	120	10	None	Compressive force
JD5-H140-T10-RY-C	140	120	140	10	Yes	Compressive force
JD6-H120-T08-RN-T	140	124	120	8	None	Tensile force
JD7-H160-T08-RN-T	180	164	160	8	None	Tensile force
JD8-H120-T08-RY-T	140	124	120	8	Yes	Tensile force

rectangular tube for applying load, as shown in Fig. 2(f). M20 high strength bolts were adopted in the bolted ball-cylinder joint. The dimensions of the concave endplate and the convex washer are plotted in Figs. 2(c) and (d). The diameter of endplate arc was the same with the outside diameter d_1 of the corresponding hollow cylinder, while the diameter of washer arc was the same with the inside diameter d_2 of the corresponding hollow cylinder. To fix the high strength bolts, threaded holes were applied. The welding material used for connecting rectangular tubes with endplates is E43 which has the same strength as those corresponding components. For the joint specimens with the ribbed stiffener, the width and thickness of the ribbed stiffener are 20 mm and 12 mm respectively, as shown in Fig. 2(b).

Five primary parameters were varied in these joint specimens, including the outside diameter of hollow cylinders d_1 , the height of hollow cylinders H , the thickness of hollow cylinders, ribbed stiffener and axial force. Detailed information of these parameters is listed in Table 1. In addition, concise symbols were assigned to these bolted ball-cylinder joint specimens for an explicit understanding. Taking the joint specimens “JD5-H140-T10-RY-C” and “JD7-H160-T08-RN-T” for example, “JD” represents the identification number of the joint specimen; “H” represents the height of the hollow cylinder; “T” represents the thickness of the hollow cylinder; “RY” indicates that the joint specimen is enhanced by the ribbed stiffener; “RN” represents the normal joint specimen without the ribbed stiffener, as shown in Fig. 2(a); “C” and “T” mean that the joint specimen is subjected to axial compressive force and axial tensile force, respectively.



(a) Test specimen without ribbed stiffener



(b) Test specimen with ribbed stiffener

Fig. 3 Bolted ball-cylinder joint specimens

3.2 Materials

All the ball-cylinder nodes and the rectangular tubes were made of mild steel Q235 (mild structural steel, the yield stress of which is 235 Mpa), while the material grade of the high strength bolts was 10.9 (2003). Tensile tests were carried out to investigate their actual mechanical properties according to the Chinese mechanical testing standard (2002). Six tensile coupons were cut directly from the core of a cylinder. All the tensile coupons had the same dimensions, as plotted in Fig. 4. The results of the tensile tests are shown in Fig. 5. The mechanical properties of these tensile coupons obtained from the tensile tests are listed in Table 2, where E is the elastic

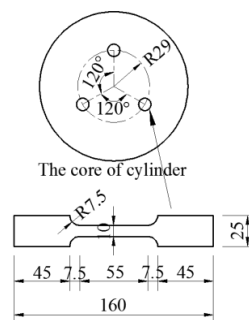


Fig. 4 Dimensions of the tensile coupons

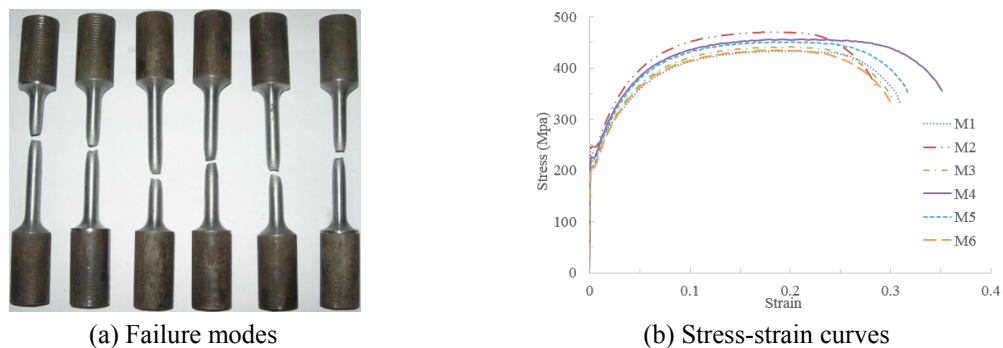


Fig. 5 Results of the tensile tests

Table 2 Mechanical properties of material

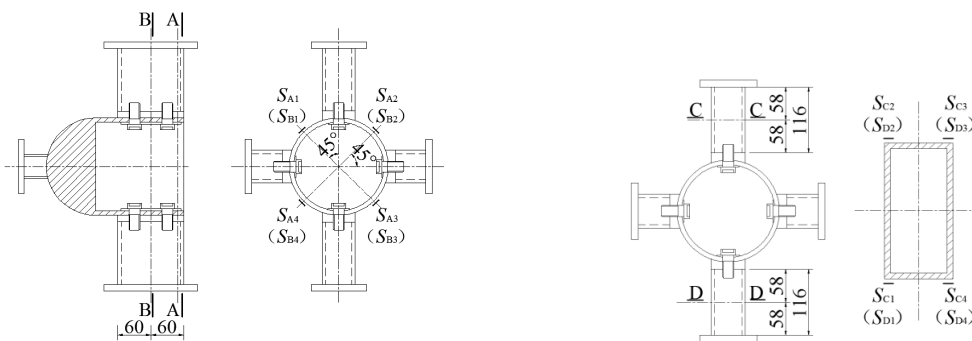
Tensile coupons	E (MPa)	f_y (MPa)	f_u (MPa)	δ_5 (%)
M1	233554	224.49	435.20	31.00
M2	196785	242.75	472.57	28.58
M3	198841	212.43	442.83	30.27
M4	203056	222.00	457.69	35.21
M5	200319	202.01	453.64	31.73
M6	224512	202.04	436.42	29.97
Average	209511	215.67	449.73	31.13

modulus, f_y is the yield strength, f_u is the ultimate tensile strength and δ_5 is the percentage elongation after fracture.

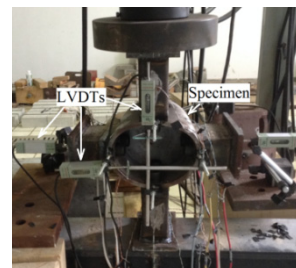
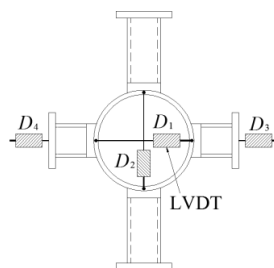
3.3 Strain and displacement measurements

The measuring points arranged for these bolted ball-cylinder joint specimens can be classified into three categories:

- (1) Hoop strain gauges placed at the hollow cylinder are plotted in Fig. 6(a). Four strain gauges ($S_{A1} \sim S_{A4}$) were located at the datum plane A, while four strain gauges ($S_{B1} \sim S_{B4}$) were located at the datum plane B. The angle between the hoop strain gauge and the rectangular tube is 45 degrees. According to the hoop strains of the hollow cylinder, the stress distributions of the hollow cylinder can be deduced.
- (2) Axial strain gauges placed at the middle of the rectangular tube are illustrated in Fig. 6(b). Four axial strain gauges ($S_{C1} \sim S_{C4}$ or $S_{D1} \sim S_{D4}$) were located at the flanges of each loaded rectangular tube. Based on the axial strains of the loaded rectangular tube, the axial force can be calculated. The axial strain gauges could be used to monitor eccentric action, and also used to validate the axial force during loading process.
- (3) In order to measure the relative deformation of the hollow cylinder, two orthogonal linear variable differential transducers (LVDTs: D_1 and D_2) were placed at the cylinder opening, as shown in Fig. 6(c). On the basis of the axial force and the deformation of the hollow cylinder, the axial stiffness and ultimate bearing capacities of these bolted ball-cylinder joint specimens can be calculated. In addition, two horizontal LVDTs (D_3 and D_4) were

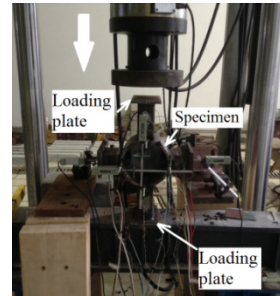
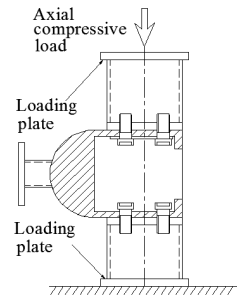


(a) Hoop strain gauges placed at the hollow cylinder (b) Axial strain gauges placed at the rectangular tube

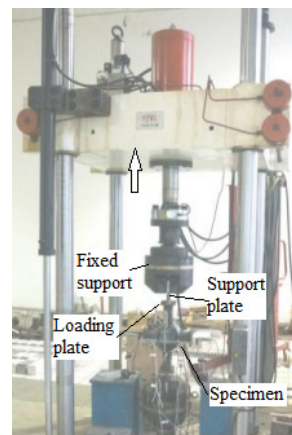
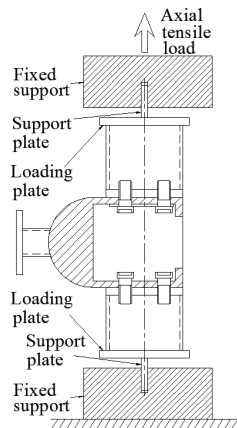


(c) LVDTs

Fig. 6 Arrangements for measuring points



(a) Axial compressive force



(b) Axial tensile force

Fig. 7 Loading schemes

placed at the end of each unloaded tube to observe the horizontal deformation of these joint specimens.

3.4 Loading schemes

The objective of this experimental program is to provide insight into the mechanical behaviour of bolted ball-cylinder joints. Thereby, five bolted ball-cylinder joint specimens were under axial compressive force, while another three bolted ball-cylinder joint specimens were under tensile force. For axial compressive tests, the loading plate should be flat so that the joint specimens could be placed on the loading system easily and stably, as shown in Fig. 7(a). For axial tensile tests, one support plate was welded at each loading plate for applying tensile load. To transfer the tensile force stably, fixed supports were adopted. Furthermore, they infibulated the support plates tightly. The axial tensile force was applied to the fixed support, as shown in Fig. 7(b).

3.4 Loading schemes

The objective of this experimental program is to provide insight into the mechanical behaviour of bolted ball-cylinder joints. Thereby, five bolted ball-cylinder joint specimens were under axial compressive force, while another three bolted ball-cylinder joint specimens were under tensile



Fig. 8 Test process

force. For axial compressive tests, the loading plate should be flat so that the joint specimens could be placed on the loading system easily and stably, as shown in Fig. 7(a). For axial tensile tests, one support plate was welded at each loading plate for applying tensile load. To transfer the tensile force stably, fixed supports were adopted. Furthermore, they infibulated the support plates tightly. The axial tensile force was applied to the fixed support, as shown in Fig. 7(b).

4. Failure modes and bearing capacities

An overall description on the failure phenomena of all the bolted ball-cylinder joint specimens is listed in Table 3, where P_u represents the ultimate load. The failure modes of these joint specimens are shown in Fig. 9. It is seen that failure was concentrated on the hollow cylinder, the bolt and the weld. The primary failure modes included excessive deformation at the opening of the hollow cylinder, punching failure at the wall of the hollow cylinder, evulsion of the bolt and weld cracking.

For the joint specimens subjected to axial compressive force, excessive deformation occurred at the opening of the hollow cylinder. However, the deformation of the hollow cylinder near the solid hemisphere was relative small due to the constraint of the solid hemisphere. The concave endplates connected with the unloaded rectangular tubes were detached from the hollow cylinder obviously,

Table 3 Failure modes of the test specimens

No.	Failure modes	P_u (kN)
JD1-H140-T10-RN-C	Excessive deformation at the opening of the hollow cylinder	341.60
JD2-H160-T12-RN-C	Excessive deformation at the opening of the hollow cylinder	391.68
JD3-H120-T12-RN-C	Excessive deformation at the opening of the hollow cylinder	446.00
JD4-H120-T10-RN-C	punching failure at the wall of the hollow cylinder	349.20
JD5-H140-T10-RY-C	Excessive deformation at the opening of the hollow cylinder	440.60
JD6-H120-T08-RN-T	Weld cracking	167.70
JD7-H160-T08-RN-T	Evulsion of the bolts; excessive deformation at the opening of the hollow cylinder; weld cracking	178.40
JD8-H120-T08-RY-T	Weld cracking; inconspicuous deformation of the hollow cylinder	186.10

as shown in Figs. 9(a)~(c). Besides, an indentation was created at the hollow cylinder because of the compressive force. Moreover, the indentation near the solid hemisphere was deeper than the one near the opening. It is worth noting that when the thickness of the hollow cylinder was very thin, the punching failure occurred (JD4-H120-T10-RN-C).



(a) JD1-H140-T10-RN-C



(b) JD2-H160-T12-RN-C



(c) JD3-H120-T12-RN-C



(d) JD4-H120-T10-RN-C



(e) JD5-H140-T10-RY-C



Fig. 9 Failure modes



(f) JD6-H120-T08-RN-T



(g) JD7-H160-T08-RN-T



(h) JD8-H120-T08-RY-T



Fig. 9 Continued

For the joint specimens subjected to axial tensile force, the hollow cylinder was deformed because of the tensile force. Then, the concave endplates connected with the loaded rectangular tubes was detached from the hollow cylinder obviously, as shown in Figs. 9(f)~(h). Finally, these joint specimens were failed with weld cracking. It is worth noting that when the outside diameter of the hollow cylinder is very large, the evulsion of the bolt occurred (JD7-H160-T08-RN-T).

4.1 Effect of the dimensions of the hollow cylinder

The thickness of the hollow cylinder has a significant effect on the failure modes and bearing capacities of bolted ball-cylinder joints. With respect to the joint specimens JD1 and JD2, the ultimate load improved by 14.7% when the thickness of the hollow cylinder increased from 10 mm to 12 mm. With respect to the joint specimens JD3 and JD4, the ultimate load improved by 27.7% when the thickness of the hollow cylinder increased from 10 mm to 12 mm.

Only the joint specimen JD4 was failed with the punching damage at the wall of the hollow cylinder. The primary reasons for this may be: (1) the thickness of the hollow cylinder was thin, leading to a low shearing capacity of the hollow cylinder; (2) the height of the hollow cylinder was short. Therefore, the deformation of the hollow cylinder near the solid hemisphere was limited strongly. To release the energy, the punching failure occurred.

The evulsion of the bolt only occurred at the joint specimen JD7. The main reason may be that the larger the outside diameter is, the more flexible the hollow cylinder is

4.2 Effect of the ribbed stiffener

Regarding the compression joint specimens JD1 and JD5, which only differ in the ribbed stiffener, the experimental results shows that with the help of the ribbed stiffener, the ultimate load of the bolted ball-cylinder joint was 29% greater than the one without the ribbed stiffener. Since the ribbed stiffener enhanced the joint compressive stiffness evidently, the bearing capacity was improved.

Regarding the tension joint specimens JD6 and JD8 which only differ in the ribbed stiffener, the deformation of the joint specimen JD6 was large, while the deformation of the joint specimen JD8 was few. It is signified that the ribbed stiffener improves the joint tensile stiffness significantly. The ultimate load of the bolted ball-cylinder joint with the ribbed stiffness was 11% greater than that without the ribbed stiffener. The main reason may be that the excessive deformation resulted in the nonuniform stress distributions. It is observed that the weld of the joint specimen JD6 was cracked at the bottom of the rectangular tube, as shown in Fig. 9(f), while the weld of the joint specimen JD8 was cracked at the whole cross-section of the rectangular tube, as shown in Fig. 9(h).

4.3 Effect of the loading schemes

The primary failure modes of the joint specimens subjected to axial compressive force were the excessive deformation and punching failure of the hollow cylinder, whereas the primary collapse mechanisms of the joint specimens subjected to axial tensile force included the evulsion of the bolt and the weld cracking. It is observed that the ultimate loads of the compression joint specimens were much higher than that of the tension joint specimens due to the different failure modes. In addition, it can be concluded that the failure modes and bearing capacities of the compression joint specimens were mainly controlled by the dimensions of the hollow cylinder, while the failure modes and bearing capacities of the tension joint specimens were mainly controlled by the bolt and weld connections.

5. Strain distributions and axial stiffness

5.1 Load-strain curves of the rectangular tube

According to the axial strains of the loaded rectangular tube, the axial force can be calculated as follows

$$F_{C-C} = \frac{1}{4}(\varepsilon_{C1} + \varepsilon_{C2} + \varepsilon_{C3} + \varepsilon_{C4})EA \quad (1)$$

$$F_{D-D} = \frac{1}{4}(\varepsilon_{D1} + \varepsilon_{D2} + \varepsilon_{D3} + \varepsilon_{D4})EA \quad (2)$$

Where $\varepsilon_{C1} \sim \varepsilon_{C4}$ and $\varepsilon_{D1} \sim \varepsilon_{D4}$ represent the axial strains located at the C-C cross-section and the D-D cross-section (Fig. 6) of the loaded rectangular tube, respectively; E is the elastic modulus; A is the cross-section area of the loaded rectangular tube.

The load-displacement curves of the loaded rectangular tube are shown in Fig. 10. Calculated curves agree very well with test curves at the initial stage of the loading process. This implies the reliability and validity of the experimental results.

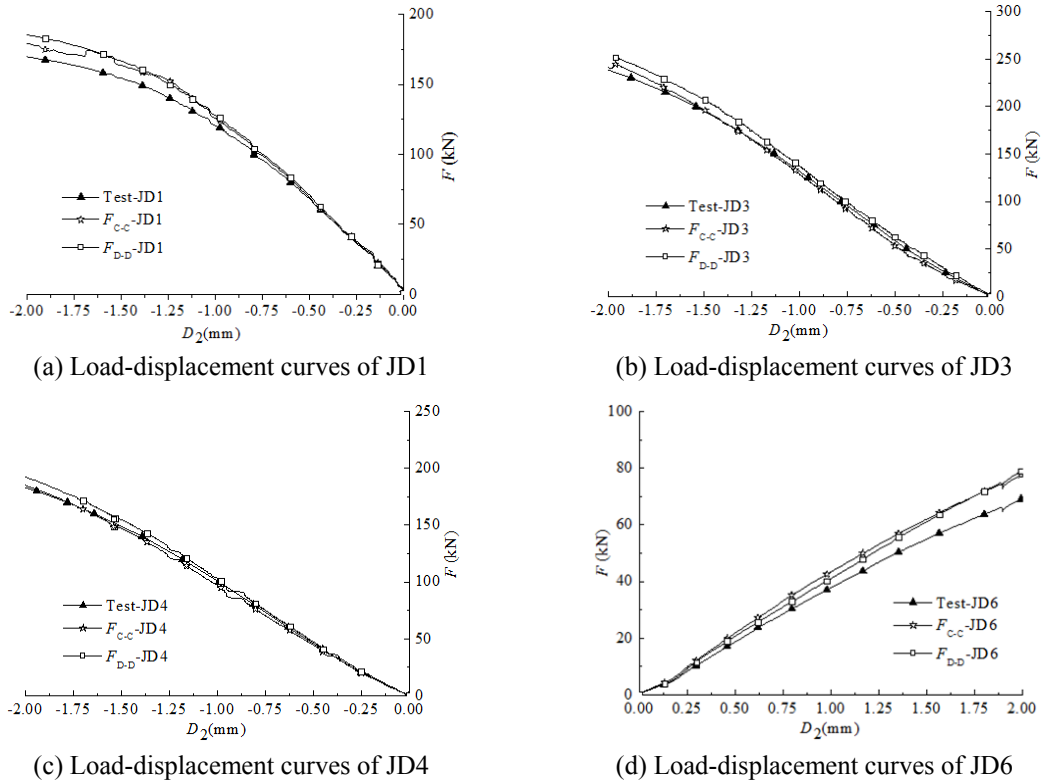


Fig. 10 Load-displacement curves of the loaded rectangular tube

5.2 Load-strain curves of the hollow cylinder

The load-strain curves of the hollow cylinder are plotted in Figs. 11~12.

Figs. 11(a)~(c) exhibit the variations of the hoop strains near the hollow cylinder opening of the joint specimens JD1, JD3 and JD4, respectively. According to the deformation of the joint specimens subjected to axial compressive force, bending moments acting on the hollow cylinder can be deduced, as drawn in Fig. 13(a). Due to the influence of the positive bending moment, compressive stress is generated at the outside surface of the hollow cylinder, and tensile stress is generated at the inside surface of the hollow cylinder. On the contrary, the influence of the negative bending moment is opposite to that of the positive bending moment. Besides, the bending moment is zero at contraflexure points. It can be evidently observed that the positive bending moment was created near the region connected with the loaded tubes, and the negative bending moment was created near the region connected with the unloaded tubes. Therefore, the hoop strain gauges were quite close to the contraflexure points. At the beginning of the loading process, the strain distributions were complicated. As the load increased, on the one hand, the hollow cylinder became flatter and flatter; on the other hand, the influence of the constraint of concave endplates became stronger and stronger. Consequently, the contraflexure points moved toward to unconstrained parts and were away from the hoop strain gauges further and further. At last, all the hoop strains expressed compressive characteristics. In addition, the hoop strains of the joint specimen JD4 were much smaller than that of the joint specimen JD3, signifying that the punching

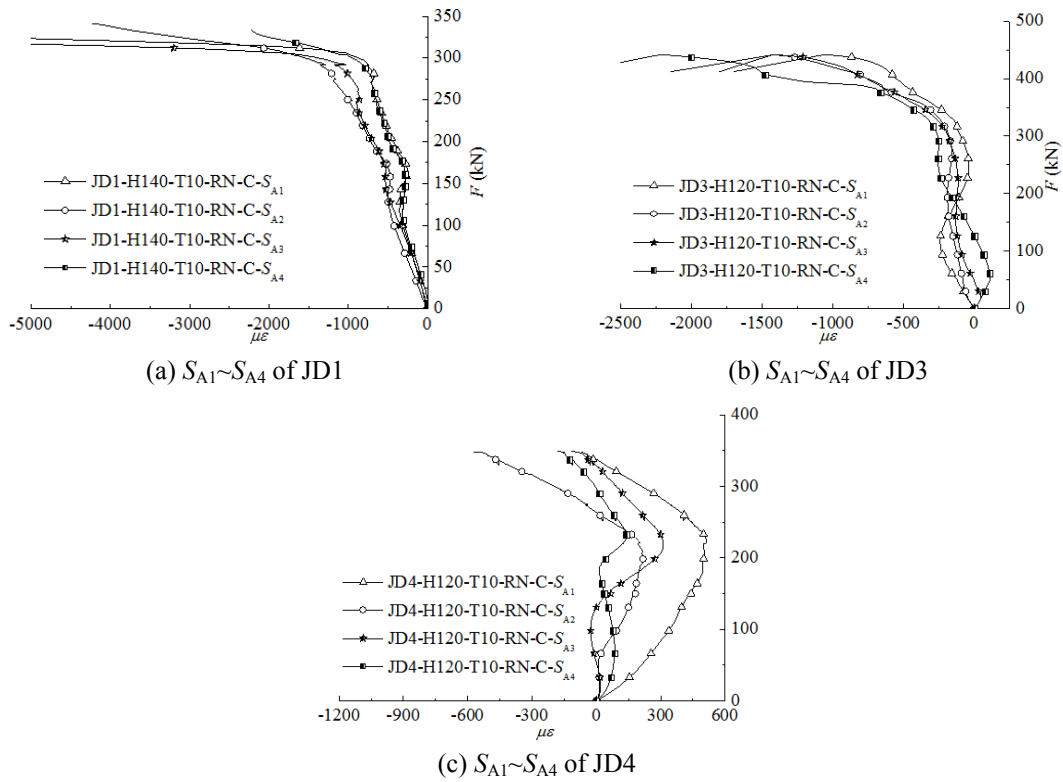


Fig. 11 Load-strain curves of the joint specimens subjected to compressive force

failure belongs to a brittle failure.

Figs. 12(a) and (b) exhibit the variations of the hoop strains near the hollow cylinder opening of the joint specimens JD6 and JD7, respectively. It can be found that the hoop strains of the tension joint specimens are larger than that of the compression joint specimens due to the thinner hollow cylinder. Their bending moments acting on the hollow cylinder is shown in Fig. 13(b). For the tension joint specimens, the positive bending moment was created near the region connected with the unloaded tubes, and the negative bending moment was created near the region connected with the loaded tubes. The conclusions obtained from the load-strain curves of the tension joint specimens were in line with that of the compression joint specimens. In addition, the hoop strain variations near the middle of the hollow cylinder of the joint specimen JD7 are plotted in Fig. 12(c).

It is evident that when the bolted ball-cylinder joint was subjected to unidirectional compressive force or tensile force, the strain distributions of the hollow cylinder were mainly controlled by the bending moment. Meanwhile, they were influenced by the constraint of concave endplates. In addition, the variation tendencies of the central symmetrical strains were the same during the whole range of the loading process.

5.3 Load-displacement curves

According to the relative deformation measured by the LVDT D_2 , load- D_2 curves were obtained. The load- D_2 curves of the joint specimens subjected to compressive force and tensile force are

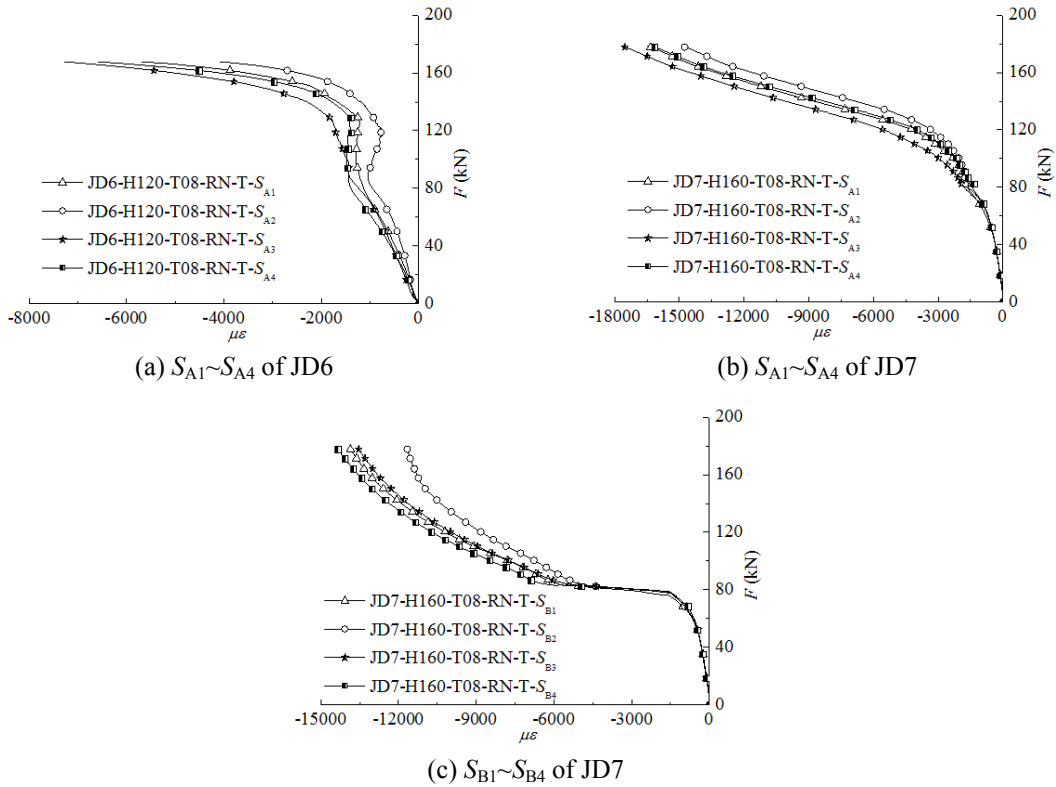


Fig. 12 Load-strain curves of the joint specimens subjected to tensile force

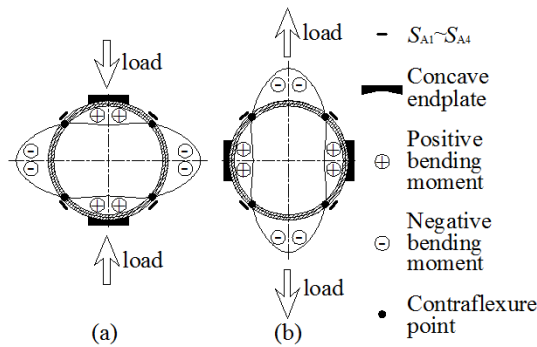


Fig. 13 Bending moments acting on the hollow cylinder

plotted in Figs. 14 and 15, respectively. To obtain their initial axial stiffness, linear regression analysis is used in the elastic phase. The values of the initial axial stiffness are listed in Table 4.

During the loading process, these joint specimens approximately went through two phases. At the beginning of the loading process, the axial stiffness presented the elastic behaviour. As the load increased, the hollow cylinder entered into the plastic phase gradually, resulting in the rapid decrease of the axial stiffness.

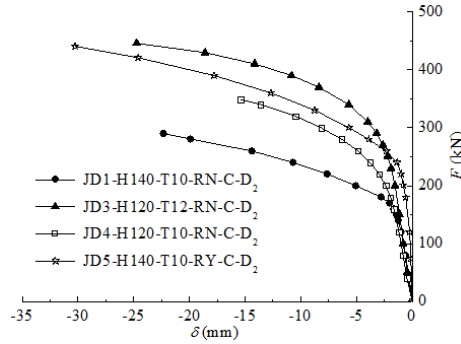
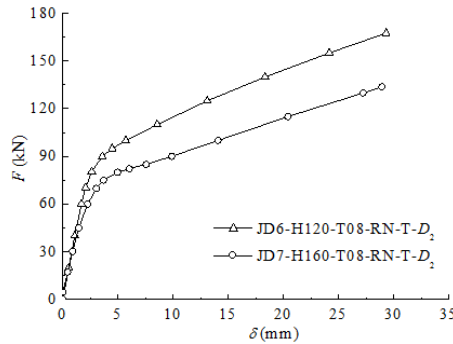
Fig. 14 Load- D_2 curves of the joint specimens subjected to compressive forceFig. 15 Load- D_2 curves of the joint specimens subjected to tensile force

Table 4 Initial axial stiffness of the specimens (kN/mm)

No.	Initial axial stiffness	No.	Initial axial stiffness
JD1	104.07	JD5	504.05
JD3	121.62	JD6	34.40
JD4	96.13	JD7	27.79

The thickness of the hollow cylinder plays a key role in the initial axial stiffness of bolted ball-cylinder joints. For the joint specimens JD3 and JD4, the initial compressive stiffness improved by 26.52% as the thickness of the hollow cylinder increased from 10 mm to 12 mm. The outside diameter of the hollow cylinder also has an important effect on the initial axial stiffness of bolted ball-cylinder joints. For the compression joint specimens JD1 and JD4, the initial compressive stiffness weakened by 7.63% as the outside diameter of the hollow cylinder increased from 140 mm to 180 mm. For the tension joint specimens JD6 and JD7, the initial tensile stiffness weakened by 19.22% as the outside diameter of the hollow cylinder increased from 140 mm to 180 mm. Therefore, it can be found that the thicker and smaller the hollow cylinder is, the stiffer the axial stiffness is.

The ribbed stiffener can effectively enhance the initial axial stiffness of bolted ball-cylinder joints. With the help of ribbed stiffener, the initial compressive stiffness of the joint specimen JD5

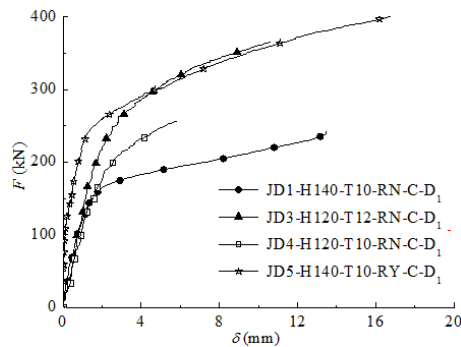


Fig. 16 Load- D_1 curves of the joint specimens subjected to compressive force

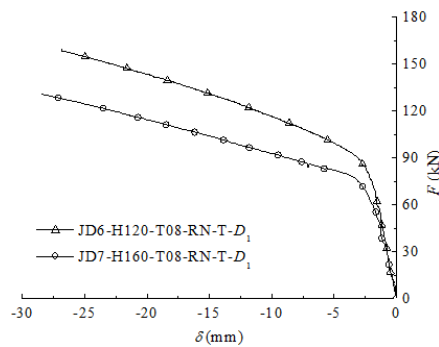


Fig. 17 Load- D_1 curves of the joint specimens subjected to tensile force

was 384.34% greater than the one of the specimen JD1. The primary reason for this may be because the ribbed stiffener limits the deformation of the hollow cylinder opening significantly.

According to the relative deformation measured by the LVDT D_1 , the load- D_1 curves were obtained. The load- D_1 curves of the joint specimens subjected to compressive force and tensile force are plotted in Figs. 16 and 17, respectively. The relative deformation measured by the LVDT D_1 was usually smaller than the corresponding one measured by the LVDT D_2 . It is obviously observed that the orthogonal deformation measured by the LVDTs D_1 and D_2 was opposite. Therefore, the axial stiffness of bolted ball-cylinder joints might be weakened by the opposite orthogonal force, but might be improved by the same orthogonal force. In addition, the similar conclusions on the axial stiffness of bolted ball-cylinder joints were obtained according to the load- D_1 curves.

6. Conclusions

Full-scale experiments on eight bolted ball-cylinder joint specimens subjected to axial force are reported in this paper. The main conclusions could be drawn from the experimental results as follows:

- (1) The failure was concentrated on the hollow cylinder, the bolt and the weld. The primary failure modes included excessive deformation at the opening of the hollow cylinder,

- punching failure at the wall of the hollow cylinder, evulsion of the bolt and weld cracking.
- (2) For the compression joint specimens, the main failure mode was the excessive deformation at the opening of the hollow cylinder. However, when the thickness of the hollow cylinder was very thin or the height of the hollow cylinder was very short, the punching failure occurred. The failure modes of the compression joint specimens were mainly controlled by the dimensions of the hollow cylinder.
 - (3) For the tension joint specimens, the main failure mode was the weld cracking. However, when the outside diameter of the hollow cylinder was very large, the evulsion of the bolt occurred. The failure modes of the tension joint specimens were mainly controlled by the bolt and weld connections.
 - (4) To improve the ultimate bearing capacity and the axial stiffness of the bolted ball-cylinder joint, two effective measures were developed. On the one hand, the thickness of hollow cylinder needed to be thicker; on the other hand, the ribbed stiffener placed at the hollow cylinder opening should be considered.
 - (5) The strain distributions of the hollow cylinder were mainly controlled by the bending moment. For the compression joint specimens, the positive bending moment was created near the region connected with the loaded tubes, and the negative bending moment was created near the region connected with the unloaded tubes. The bending moment acting on the hollow cylinder of the tension joint specimens was opposite to that of the compression joint specimens. In addition, the strain distributions were also influenced by the constraint of concave endplates.
 - (6) Both the thicker hollow cylinder and the ribbed stiffener could improve the joint axial stiffness significantly. However, the larger outsider diameter of the hollow cylinder might weaken the axial stiffness. In addition, the axial stiffness of bolted ball-cylinder joints might be weakened by the opposite orthogonal force, but might be improved by the same orthogonal force.

The bolted ball-cylinder joint has a widespread application prospect. This experimental study has offered a comprehensive understanding on the failure modes, bearing capacities and axial stiffness of bolted ball-cylinder joints. For the practical application and development, further studies including the finite element simulations and theoretical analyses are required.

Acknowledgments

The authors gratefully acknowledge the financial support provided by Natural Science Foundation of China under Grant No. 50908168 and No. 51478335. The authors would like to thank Linlin Liu for excellent technical support.

References

- Cabrero, J.M. and Bayo, E. (2007a), "The semi-rigid behaviour of three-dimensional steel beam-to-column steel joints subjected to proportional loading. Part I. Experimental evaluation", *J. Construct. Steel Res.*, **63**(9), 1241-1253.
- Cabrero, J.M. and Bayo, E. (2007b), "The semi-rigid behaviour of three-dimensional steel beam-to-column steel joints subjected to proportional loading. Part II: Theoretical model and validation", *J. Construct. Steel Res.*, **63**(9), 1254-1267.

- Daniūnas, A. and Urbonas, K. (2008), "Analysis of the steel frames with the semi-rigid beam-to-beam and beam-to-column knee joints under bending and axial forces", *Eng. Struct.*, **30**(11), 3114-3118.
- Ebadi, M. and Davoodi, M. (2012), "Evaluate Axial Stiffness of the MERO Connection, Under the Effect of Hardening the Screw", *Int. J. Sci. Emerg. Technol.*, **4**(1), 116-122.
- Fan, F., Ma, H.H., Chen, G.B. and Shen, S.Z. (2012), "Experimental study of semi-rigid joint systems subjected to bending with and without axial force", *J. Construct. Steel Res.*, **68**(1), 126-137.
- Fung, T.C., Soh, C.K. and Gho, W.M. (2001a), "Ultimate capacity of completely overlapped tubular joints II: Behavioural study", *J. Construct. Steel Res.*, **57**(8), 881-906.
- Fung, T.C., Soh, C.K., Gho, W.M. and Qin, F. (2001b), "Ultimate capacity of completely overlapped tubular joints I: An experimental investigation", *J. Construct. Steel Res.*, **57**(8), 855-880.
- GB 50017-2003 (2003), Code for design of steel structures; Ministry of housing and urban-rural development of the people's republic of China, General administration of quality supervision, inspection and quarantine of the people's republic of China. [In Chinese]
- GB/T 228-2002 (2002), Metallic materials-Tensile testing at ambient temperature; Ministry of housing and urban-rural development of the people's republic of China, General administration of quality supervision, inspection and quarantine of the people's republic of China. [In Chinese]
- Ghasemi, M., Davoodi, M.R. and Mostafavian, S.A. (2010), "Tensile Stiffness of MERO-Type Connector Regarding Bolt Tightness", *J. Appl. Sci.*, **10**(9), 724-730.
- Gil, B. and Bayo, E. (2008a), "An alternative design for internal and external semi-rigid composite joints. Part I: Experimental research", *Eng. Struct.*, **30**(1), 218-231.
- Gil, B. and Bayo, E. (2008b), "An alternative design for internal and external semi-rigid composite joints. Part II: Finite element modelling and analytical study", *Eng. Struct.*, **30**(1), 232-246.
- Guo, X.N., Xiong, Z., Luo, Y.F., Qiu, L.Q. and Huang, W.J. (2015a), "Application of the component method to aluminum alloy gusset joints", *Adv. Struct. Eng.*, **18**(11), 1845-1858.
- Guo, X.N., Xiong, Z., Luo, Y.F., Qiu, L.Q. and Liu, J. (2015b), "Experimental investigation on the semi-rigid behavior of aluminium alloy gusset joints", *Thin-Wall. Struct.*, **87**, 30-40.
- Guo, X.N., Xiong, Z., Luo, Y.F., Xu, H. and Liang, S.P. (2016a), "Block tearing and local buckling of aluminum alloy gusset joint plates", *KSCE J. Civil Eng.*, **20**(2), 820-831.
- Guo, X.N., Huang, Z.W., Xiong, Z., Yang, S.F. and Peng, L. (2016b), "Numerical studies on behaviour of bolted ball-cylinder joint under axial force", *Steel Compos. Struct., Int. J.*, **20**(6), 1323-1343.
- Han, Q.H. and Liu, X.L. (2004), "Ultimate bearing capacity of the welded hollow spherical joints in spatial reticulated structures", *Eng. Struct.*, **26**(1), 73-82.
- Kattner, M. and Crisinel, M. (2000), "Finite element modelling of semi-rigid composite joints", *Comput. Struct.*, **78**(1-3), 341-353.
- Lesani, M., Bahaari, M.R. and Shokrieh, M.M. (2013), "Detail investigation on un-stiffened T/Y tubular joints behavior under axial compressive loads", *J. Construct. Steel Res.*, **80**(4), 91-99.
- Lima, L.R.O., Andrade, S.A.L., da S. Vellasco, P.C.G. and da Silva, L.S. (2002), "Experimental and mechanical model for predicting the behaviour of minor axis beam-to-column semi-rigid joints", *Int. J. Mech. Sci.*, **44**(6), 1047-1065.
- Lopez, A., Puente, I. and Aizpurua, H. (2011), "Experimental and analytical studies on the rotational stiffness of joints for single-layer structures", *Eng. Struct.*, **33**(3), 731-737.
- Ma, H.H., Fan, F., Chen, G.B. and Shen, S.Z. (2013), "Numerical analyses of semi-rigid joint systems subjected to bending with and without axial force", *J. Construct. Steel Res.*, **90**, 13-28.
- Qiang, X.H., Bijlaard, F.S.K., Kolstein, H. and Jiang, X. (2014a), "Behaviour of beam-to-column high strength steel endplate connections under fire conditions - Part 1: Experimental study", *Eng. Struct.*, **64**, 23-38.
- Qiang, X.H., Bijlaard, F.S.K., Kolstein, H. and Jiang, X. (2014b), "Behaviour of beam-to-column high strength steel endplate connections under fire conditions - Part 2: Numerical study", *Eng. Struct.*, **64**, 39-51.
- Qiu, G.Z. and Zhao, J.C. (2009), "Analysis and calculation of axial stiffness of tubular X - joints under compression on braces", *J. Shanghai Jiaotong Univ.*, **14**(4), 410-417.

- Wang, X., Dong, S.L. and Wang, H.Y. (2000), "Finite element analysis of welded spherical joints' stiffness", *J. Zhejiang Univ. (Engineering Science)*, **34**(1), 77-82.
- Wang, W.Y., Li, G.Q. and Dong, Y.L. (2007), "Experimental study and spring-component modeling of extended end-plate joints in fire", *J Construct. Steel Res.*, **63**(8), 1127-1137.

CC